JCB Article

Ca^{2+}-controlled competitive diacylglycerol binding of protein kinase C isoenzymes in living cells

Johannes C. Lenz,[1] H. Peter Reusch,[2] Nadine Albrecht,[1] Günter Schultz,[1] and Michael Schaefer[1]

[1]Institut für Pharmakologie and [2]Institut für Klinische Pharmakologie und Toxikologie, Freie Universität Berlin, 14195 Berlin, Germany

The cellular decoding of receptor-induced signaling is based in part on the spatiotemporal activation pattern of PKC isoforms. Because classical and novel PKC isoforms contain diacylglycerol (DAG)-binding C1 domains, they may compete for DAG binding. We reasoned that a Ca^{2+}-induced membrane association of classical PKCs may accelerate the DAG binding and thereby prevent translocation of novel PKCs. Simultaneous imaging of fluorescent PKC fusion proteins revealed that during receptor stimulation, PKCα accumulated in the plasma membrane with a diffusion-limited kinetic, whereas translocation of PKCε was delayed and attenuated. In BAPTA-loaded cells, however, a selective translocation of PKCε, but not of coexpressed PKCα, was evident. A membrane-permeable DAG analogue displayed a higher binding affinity for PKCε than for PKCα. Subsequent photolysis of caged Ca^{2+} immediately recruited PKCα to the membrane, and DAG-bound PKCε was displaced. At low expression levels of PKCε, PKCα concentration dependently prevented the PKCε translocation with half-maximal effects at equimolar coexpression. Furthermore, translocation of endogenous PKCs in vascular smooth muscle cells corroborated the model that a competition between PKC isoforms for DAG binding occurs at native expression levels. We conclude that Ca^{2+}-controlled competitive DAG binding contributes to the selective recruitment of PKC isoforms after receptor activation.

Introduction

PKC isoenzymes form a family of serine/threonine kinases that are grouped into classical (PKCα, β1, β2, and γ), novel (PKCδ, ε, η, and θ), and atypical (PKCζ and ι/λ) isoenzymes based on their structural similarities and cofactor requirements (Nishizuka, 1992; Mellor and Parker, 1998; Ron and Kazanietz, 1999). In contrast to their highly conserved COOH-terminal catalytic core domains, NH_2-terminal regulatory domains are more variable. The diacylglycerol (DAG)*-mediated activation of classical and novel PKC isoforms is accomplished by a C1 domain that contains two cysteine-rich regions as DAG-docking motifs. DAG binding fulfills a dual role by recruiting classical and novel PKCs to the membrane compartment and by weakening the interaction of an inhibitory pseudosubstrate domain with the COOH-terminal catalytic core (Oancea and Meyer, 1998). The mode of activation, therefore, relies on the DAG-induced release from an intramolecular block. In contrast to novel PKC isoforms, classical PKCs are additionally regulated by the cytosolic Ca^{2+} concentration ($[Ca^{2+}]_i$). Their C2 domains, in conjunction with the anionic phospholipid phosphatidylserine, bind two or three calcium ions (Shao et al., 1996; Sutton and Sprang, 1998; Verdaguer et al., 1999). The bound Ca^{2+} electrostatically facilitates the plasma membrane docking of classical PKC isoforms and may, thus, explain the diffusion-limited translocation kinetics and high collisional coupling efficiency of classical PKC isoforms observed either in vitro or in living cells (Nalefski and Newton, 2001; Schaefer et al., 2001).

In virtually each cell type and tissue, at least one member of the classical and one of the novel PKC isoforms are coexpressed (Wetsel et al., 1992; Dekker and Parker, 1994; Liu and Heckman, 1998). Stimulation of PLC-coupled receptors results in DAG formation and, via inositol-1,4,5-trisphosphate ($InsP_3$) receptor activation, increases the $[Ca^{2+}]_i$. One might expect that classical and novel PKC isotypes are recruited to the plasma membrane in parallel. Nonetheless, upon receptor stimulation, an isotype-selective translocation of PKCs has been observed in several cell systems (Dekker and Parker, 1994). This isotype-specific membrane translocation of PKC isoenzymes must be based on mechanisms that take effect downstream of receptor activation. Although a number of PKC-interacting proteins sequester activated PKCs to various

Address correspondence to Michael Schaefer, Institut für Pharmakologie, Freie Universität Berlin, Thielallee 67-73, 14195 Berlin, Germany. Tel.: 49-30-8445-1863. Fax: 49-30-8445-1818. E-mail: schae@zedat.fu-berlin.de

*Abbreviations used in this paper: AoSMCs, aortic smooth muscle cells; AVP, arginine-vasopressin; DAG, diacylglycerol; DOG, di-octanoyl-*s,n*-glycerol; HBS, Hepes-buffered solution; HEK, human embryonic kidney; $InsP_3$, inositol-1,4,5-trisphosphate; ROI, region of interest.

Key words: protein kinase C; diglycerides; calcium signaling; signal transduction; protein transport

compartments (Jaken and Parker, 2000), little is known about the mechanisms that control the selectivity of the initial membrane recruitment of distinct PKC isoforms, which is most likely based on a protein–lipid interaction.

We have recently shown that a Ca^{2+}-induced plasma membrane translocation of classical PKCs is a diffusion-driven and diffusion-limited binding process that is characterized by a high collisional coupling efficiency (Schaefer et al., 2001). Because both classical and novel PKCs share a DAG-binding C1 domain, the highly efficient Ca^{2+}-driven plasma membrane association of classical PKCs suggests that, by finally competing for the same acceptor, classical PKCs may prevent translocation of coexpressed novel PKCs. To observe the interplay of PKC translocations in living cells, we generated cyan and yellow fluorescent PKC fusion proteins and applied a multivariate regression algorithm that reliably dissects signals arising from multiple, spectrally overlapping fluorochromes. We provide evidence that an agonist-induced selective membrane recruitment of classical and/or novel PKC isoenzymes can result from a Ca^{2+}-controlled competitive binding to limiting plasma membrane concentrations of DAGs.

Results

Excitation and emission spectra of fluorochromes form fingerprints that can be used to discriminate a number of dyes. Taking advantage of fast monochromators and linearly scaling CCD cameras, we set up a spectral evaluation method that estimates the contribution of single fluorochromes to complex signals in dynamic, multicolor labeling experiments. Image bursts were taken at five to eight different excitation wavelengths to record the spectral characteristics of the probe. These data were then compared with spectrally resolved datasets of each isolate fluorochrome (Fig. 1 A). Because fluorescence signals of a probe are additively composed of spectra of single fluorochromes, their relative contribution to the composite signal could be estimated with a pixel-by-pixel multivariate, linear regression analysis (results for two regions of interest are depicted in Fig. 1, B and C). Spectral shifts of ~15 nm were sufficient to achieve a reliable separation of fluorochromes such as the red-shifted green (GFP-S65T) and yellow (YFP) fluorescent proteins (unpublished data). Furthermore, by dissecting signals that arise from the spectrally shifting free and Ca^{2+}-bound forms of fura-2, a rapid calibration of cytosolic Ca^{2+} concentrations could also be achieved. Using this regression-based spectral evaluation method, we synchronously coimaged receptor-induced $[Ca^{2+}]_i$ transients and the translocation of CFP and YFP fusion proteins of classical and novel PKC isotypes.

Our recent finding that the receptor-induced translocation of classical PKC isoenzymes is a Ca^{2+}-driven diffusion-limited binding process (Schaefer et al., 2001) prompted us to hypothesize that after initially attaching to the plasma membrane via interaction of the Ca^{2+}-binding C2 domain and phosphatidylserine, the subsequent search for DAGs may be restricted to a two-dimensional space. This two-step procedure of classical PKCs to scan for DAGs in the plasma membrane may be more efficient than the translocation mechanism of novel PKCs that have to undergo several collisions with the plasma membrane until they eventually hit a DAG molecule. Indeed, in transiently transfected human embryonic kidney (HEK) cells, YFP-tagged PKCα translocated to the plasma membrane in response to maximal stimulation of a cotransfected histamine H_1 receptor, whereas coexpressed CFP-fused PKCε remained mostly cytosolic (Fig. 2, A and C). This effect was not due to massive discrepancies in the expression levels of the coexpressed PKC isoforms because the molar ratio between PKCα–YFP and PKCε–CFP was ~1:1.5, as detected by fluorescence intensities of the respective tags and a calibration procedure with an

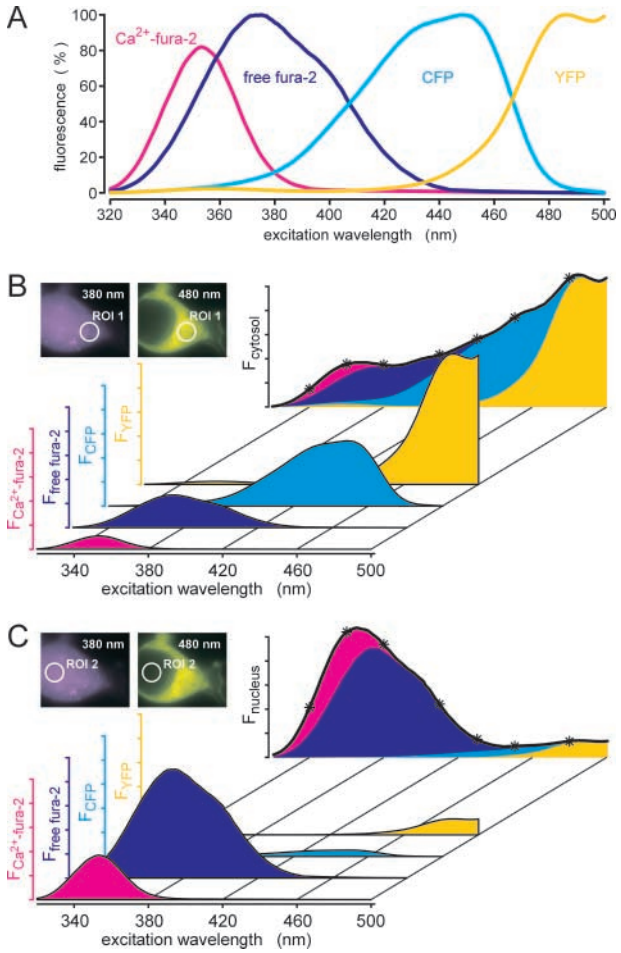

Figure 1. **Spectral deconvolution of overlapping fluorochromes eliminates cross-bleeding between multiple fluorochromes.** (A) Excitation spectra of single fluorochromes were recorded by digital fluorescence microscopy. Spectra of Ca^{2+}-bound fura-2 and free fura-2 were obtained in HEK cells after equilibration with ionomycin (10 μM for 3 h) in the presence (Ca^{2+}–fura-2) and absence (free fura-2) of external Ca^{2+}, respectively. Excitation spectra of CFP and YFP were acquired after transient expression of the respective fluorescent protein in HEK cells. All spectra were normalized to the maximal fluorescence intensities of the respective dye. (B and C) Due to differential distribution of fluorescent molecules in different regions of interest (ROI) corresponding to the peripheral cytosol (B) or the nucleus (C), cross-bleeding of fluorochromes frequently accounts for a major portion of the signals at a given excitation wavelength. The spectrum over the respective area ($F_{cytosol}$ or $F_{nucleus}$) is additively composed of signals arising from single fluorochromes ($F_{Ca2+–fura-2}$, $F_{free\ fura-2}$, F_{CFP}, and F_{YFP}). The relative contribution of each fluorochrome to the composite spectrum of the probe was calculated by a regression-based spectral evaluation algorithm.

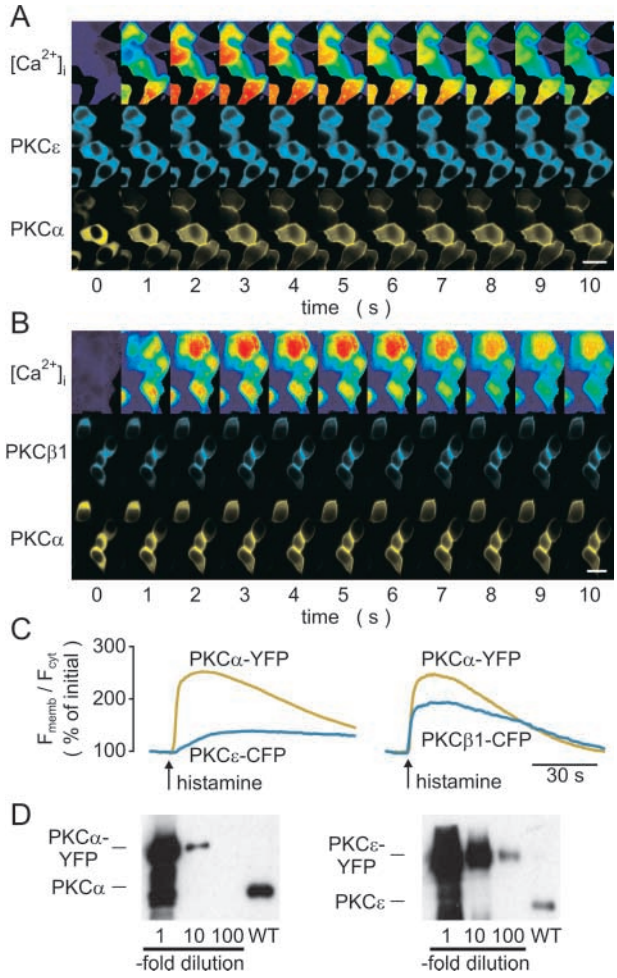

Figure 2. **PKCα suppresses a receptor-induced plasma membrane translocation of PKCε.** (A) Transiently transfected HEK cells were stimulated via a coexpressed H_1 histamine receptor (histamine 100 μM), and fluorescences were recorded at multiple excitation wavelengths (340, 360, 380, 410, 430, 450, and 480 nm) at the indicated time points after agonist application. Image data were processed by a pixel-by-pixel regression-based spectral evaluation algorithm to dissect signals arising from CFP and YFP and to calibrate $[Ca^{2+}]_i$. The calibrated $[Ca^{2+}]_i$ is encoded by a rainbow pseudocolor scale (0–1,000 nM). Note the poor translocation of PKCε and the coincident $[Ca^{2+}]_i$ elevation and translocation of PKCα. (B) Simultaneous imaging of the histamine-induced translocation of PKCα–YFP and PKCβ1–CFP. Bars, 20 μm. (C) Time-course of translocation of PKC fusion proteins from the experiments shown in A and B. For explanation of the assay, see Fig. 3 legend. (D) Expression levels of transiently overexpressed PKCα–YFP and PKCε–YFP were compared with those of endogenously expressed PKC isoenzymes by immunoblot analysis. Cytosolic fractions were prepared from transiently transfected cells (transfection efficiency >50%) or from wild-type HEK cells (WT). The undiluted samples were adjusted to contain 20 μg of total protein per lane. Blots were probed with either anti-PKCα or anti-PKCε antibodies; the molecular weight of the bands correspond to the expected sizes of wild-type PKCs or the respective YFP-fused proteins.

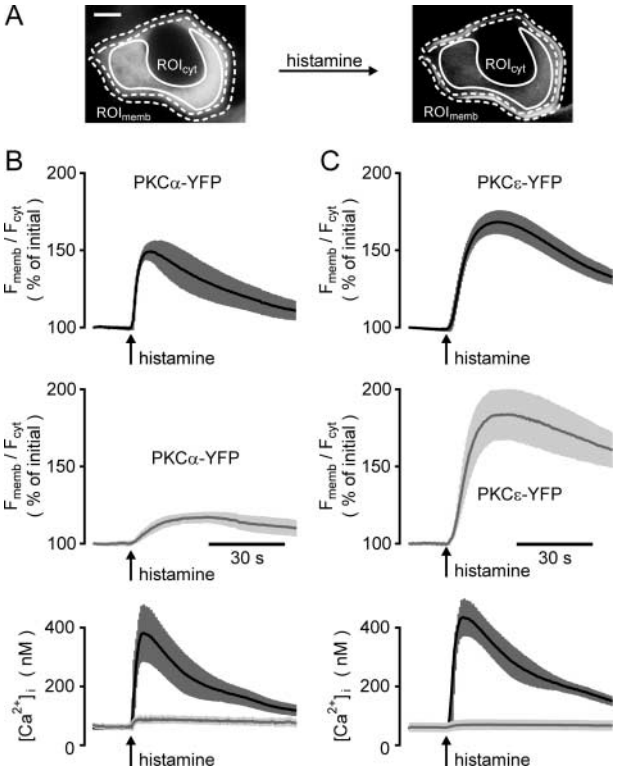

Figure 3. **Ca^{2+}-dependent collisional coupling efficiency of PKCα and PKCε.** Transiently transfected HEK cells were loaded with fura-2 and imaged by digital videomicroscopy. (A) The fluorometric determination of PKC translocation was based on the measurement of mean fluorescence intensities over ROIs that were defined over the outer border of the cell mostly representing the plasma membrane (ROI_{memb}) and over the cytosol (ROI_{cyt}) of the same cell. Bar, 5 μm. (B and C, top and middle) The receptor-induced plasma membrane translocation of PKCα–YFP (B) or PKCε–YFP (C) was monitored in HEK cells with (gray lines) or without (black lines) preincubation with BAPTA-AM (10 μM, 15 min at 37°C). HEK cells were cotransfected with plasmids encoding the indicated PKC fusion proteins and the H_1 histamine receptor. The addition of histamine (100 μM) to the bath solution is indicated by arrows. The mean fluorescence intensities (F_{memb} and F_{cyt}) were calculated for the ROI_{memb} and ROI_{cyt} of single cells, expressed as ratios, and normalized to the initial values. (B and C, bottom) $[Ca^{2+}]_i$ signals were recorded in parallel to control the efficiency of the Ca^{2+} clamp by intracellularly loaded BAPTA. Data represent means and SEM of $n = 3$–4 independent experiments (each experiment comprises averaged data of 6–15 single cells).

intramolecularly fused CFP–YFP tandem protein (see Materials and methods). Simultaneous imaging of two classical PKC isoforms, PKCα–YFP and PKCβ1–CFP (molar ratio 1:2), however, showed coincident $[Ca^{2+}]_i$ signals and simultaneous plasma membrane translocation of both PKCs (Fig. 2, B and C). Switching the fluorescent tags (PKCα–CFP coexpressed with PKCε–YFP) did not alter the impaired translocation of the novel isotype in coexpression experiments. Immunoblot analysis of endogenously expressed PKCα and PKCε along with a dilution series of transiently transfected fluorescent fusion proteins demonstrates an ~10-fold overexpression of PKCα and an ~100-fold overexpression of PKCε, as compared with endogenous expression levels (Fig. 2 D). Thus, the endogenously expressed PKC isoforms are unlikely to affect the translocation of transiently overexpressed fluorescent PKC fusion proteins. Fluorescent PKCε fusion proteins translocated in response to histamine receptor stimulation when expressed alone (Fig. 3) or when coexpressed with the unfused CFP (unpublished data), indicat-

ing that coexpressed PKCα caused the attenuation of PKCε translocation.

The initial step for the translocation of classical PKCs most likely relies on an interaction of the Ca^{2+}-binding C2 domain with phosphatidylserine. Therefore, chelation of intracellular Ca^{2+} may affect both the efficiency and the temporal pattern of PKCα translocation. To evaluate the effect of intracellularly loaded BAPTA on the kinetics of PKC translocation, the localization of fluorescent PKC fusion proteins was assessed by digital videomicroscopy and subsequent analysis of fluorescence intensities within regions of interest defined over the plasma membrane and the cytosol of single cells, as shown in Fig. 3 A. The results demonstrate that the histamine-induced plasma membrane docking of PKCα–YFP is markedly affected by BAPTA-AM pretreatment. The plasma membrane association of PKCα was delayed, and the efficiency of the binding was reduced under conditions where the formation of DAGs is the only driving force for the PKCα translocation (Fig. 3 B). The half-maximal translocation of PKCα in the absence and presence of the Ca^{2+} chelator were observed 1.2 s and 7.5 s after histamine application, respectively. The agonist-induced redistribution of the DAG-sensing PKCε–YFP remained mostly unchanged irrespective of the presence or absence of $[Ca^{2+}]_i$ transients (Fig. 3 C). Half-maximal translocation of PKCε–YFP was observed 6–7 s after histamine stimulation in untreated or in BAPTA-loaded cells. Upon buffering of $[Ca^{2+}]_i$ signals, a slight, but statistically not significant, increase in the translocation efficiencies of PKCε–YFP could be observed (Fig. 3 C, top and middle). Because the endogenous expression level of PKCα in HEK293 cells is not neglectably low (Fig. 2 D), it is possible that this paradoxical inverse Ca^{2+} sensitivity of PKCε translocation could reflect a competition with endogenous classical PKCs. Applying the spectral evaluation method, $[Ca^{2+}]_i$ could be detected in parallel to control the Ca^{2+} clamp of intracellularly loaded BAPTA in the same cells that were used to detect the PKC translocation (Fig. 3, B and C, bottom). Thus, in the absence of $[Ca^{2+}]_i$ signals, the receptor-induced PKCα translocation no longer precedes the membrane recruitment of PKCε. Furthermore, the weak and delayed translocation of PKCα–YFP in BAPTA-loaded cells indicates that PKCα may bind to DAGs with a lower affinity than the novel PKC isoform.

A possible Ca^{2+}-controlled competition for the membrane anchorage of classical and novel PKCs was tested by coexpressing CFP- and YFP-tagged PKC fusion proteins and altering the intracellular Ca^{2+} concentrations. In HEK cells coexpressing PKCα–CFP and PKCε–YFP, maximal stimulation of a coexpressed histamine receptor induced a similar translocation of PKCα (Fig. 4 A) as in cells that expressed PKCα alone (Fig. 3 B). The histamine-induced translocation of PKCε, however, was markedly delayed, and the maximal membrane attachment was reduced in cells that coexpressed PKCα as compared with cells that were not cotransfected with PKCα (Fig. 3 C; Fig. 4 A). In PKCα/PKCε-coexpressing cells, a pretreatment with BAPTA-AM reversed the selectivity of the receptor-induced PKC translocation. The histamine-induced translocation of PKCα was further suppressed, whereas the membrane association of coexpressed PKCε now remained as efficient as in cells that

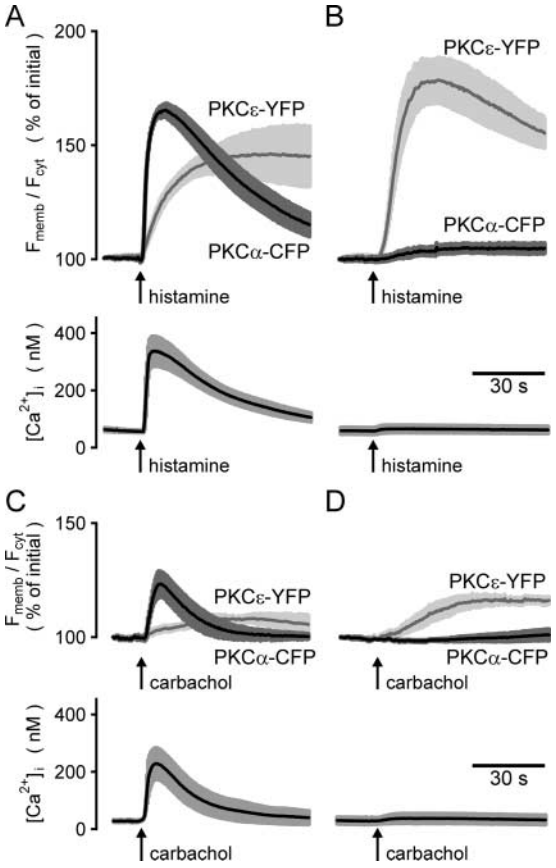

Figure 4. **A competitive translocation of PKC isoforms is controlled by $[Ca^{2+}]_i$.** The Ca^{2+} dependency of the histamine- or carbachol-induced PKC translocation was analyzed in HEK cells that were transiently transfected with PKCα–CFP, PKCε–YFP, and the H_1 histamine receptor. Cells were stimulated with either histamine (100 μM; A and B) or carbachol (20 μM; C and D) acting on an endogenously expressed M_1 family acetylcholine receptor. The agonist application is indicated by arrows. $[Ca^{2+}]_i$ elevations and translocations of the indicated PKC isoenzymes were simultaneously recorded without (A and C) or with pretreatment with 10 μM BAPTA-AM (B and D). The translocation of fluorescent PKC fusion proteins was assessed as described in Fig. 3. Data represent means and SEM of $n = 3$–5 independent experiments. In each experiment, data of 8–22 single cells were averaged.

only expressed the PKCε fusion protein (Fig. 4 B as compared with Fig. 3, B and C). In another experiment, we coexpressed the H_1 receptor together with PKCε–CFP and only trace amounts of PKCα–YFP (molar ratio between PKCε–CFP and PKCα–YFP ~5:1). Under these conditions, the histamine-induced translocation of PKCε–CFP displayed identical efficiencies and kinetics as shown for PKCε–YFP without cotransfected PKCα (Fig. 3 C).

The competitive effect was not restricted to stimulation via the coexpressed H_1 histamine receptor. When PKCα–CFP/PKCε–YFP-coexpressing HEK cells were stimulated via a coexpressed human EGF receptor (EGF, 50 ng/ml), PKCα was efficiently translocated whereas PKCε remained mostly cytosolic, and BAPTA loading again reversed the selectivity of PKC translocation (unpublished data). In PKCα/PKCε-coexpressing cells that were stimulated with submaximal effective concentrations of carbachol (20 μM)

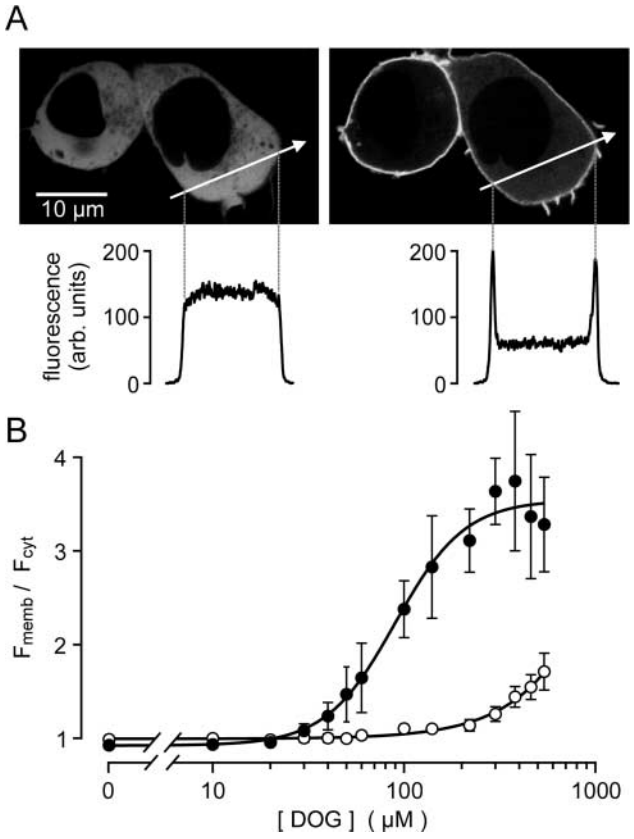

Figure 5. **Differential DAG binding affinity of PKCα and PKCε in living cells.** Fluorescent PKC fusion proteins were transiently transfected in HEK cells and challenged with various concentrations of the membrane-permeable DOG. (A) Confocal images of a PKCε–YFP-expressing cell were taken before and 60 s after application of DOG (300 μM), and fluorescence intensity profiles were recorded over the cytoplasm and the adjacent plasma membrane of single cells. (B) The mean cytosolic and plasma membrane fluorescence intensities were recorded for either PKCα (open symbols) or PKCε (filled symbols), as shown in A, and expressed as ratios. Data represent means ± SEM of five independent experiments (each experiment comprises averaged data of three to five cells).

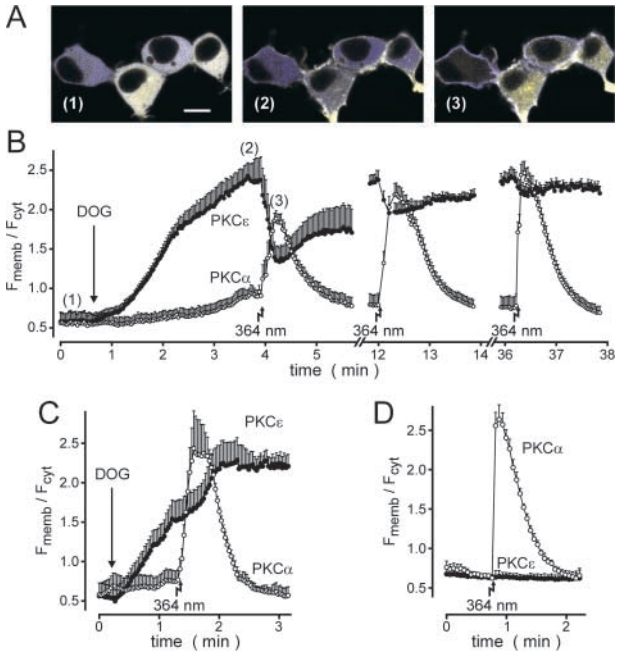

Figure 6. **PKCα and PKCε compete for DAG binding in a Ca^{2+}-dependent manner.** (A) HEK cells were transiently cotransfected with PKCα–CFP (shown in blue) and PKCε–YFP (yellow channel), loaded with caged Ca^{2+} (*o*-nitrophenyl-EGTA, 10 μM), and imaged by confocal time-lapse microscopy. Images before (1) and 3 min after (2) the addition of the membrane-permeable DOG (10 μM) are shown. Subsequently, caged Ca^{2+} was photolyzed by applying a brief pulse of maximal laser energy at 364 nm (3). Bar, 10 μm. (B) Kinetic analysis of the whole experiment shown in A. Fluorescence intensities over the plasma membrane and the cytosol are expressed as ratios and SD of four cells. Comparable cell groups were allocated on the same coverslip and subjected to photolysis of caged Ca^{2+} (as indicated by the flash symbols) at later time points. (C) Similar experiment as in B, but with separately transfected PKCε–CFP and PKCα–YFP so that each cell expresses either PKCα–YFP or PKCε–CFP. (D) Equivalent experiment as in C, but without previous addition of DOG. Representatives of three independent experiments with similar results are shown.

via an endogenously expressed M_1 family muscarinic receptor, a smaller and more short-lived $[Ca^{2+}]_i$ signal indicates a weaker input into the PLC signaling pathway as compared with the full stimulation of a coexpressed H_1 histamine receptor (Fig. 4, A and C). Under these conditions, the translocation of PKCα–CFP was still evident, whereas translocation of PKCε–YFP was poorly detectable. When carbachol-induced $[Ca^{2+}]_i$ transients were buffered by intracellular BAPTA, PKCε–YFP was translocated to the plasma membrane although the stimulation via the endogenous receptor resulted in a more delayed and weaker translocation as compared with the stimulation of the exogenously transfected H_1 receptor (Fig. 4, B and D). In the presence of $[Ca^{2+}]_i$ signals, the highly efficient membrane association of classical PKC isoforms may occupy the accessible DAG molecules and thereby displace novel PKC isoforms. In BAPTA-loaded cells, however, the remaining driving force for the histamine-, carbachol-, or EGF-induced PKC translocation of classical or novel PKCs is given by the formation of endogenous DAG species by PLC-β or -γ isoforms. Because PKCε selectively translocates to the plasma membrane under these conditions, we conclude that the novel PKC isoenzyme binds to endogenous DAG species with a higher affinity than the coexpressed PKCα.

This concept is corroborated by the finding that low concentrations (20–100 μM) of the membrane-permeable dioctanoyl-*s,n*-glycerol (DOG) selectively recruited PKCε to the plasma membrane, whereas PKCα required ~10-fold higher DOG concentrations for a comparable plasma membrane association (Fig. 5). The concentration-dependent plasma membrane association was assessed by confocal measurement of transcellular concentration profiles of PKC isoforms 60 s after the addition of DOG (Fig. 5 A). The EC_{50} for the DOG-induced membrane association of PKCε–YFP was ~90 μM, and saturation was observed at concentrations >300 μM. The fluorescent PKCα fusion protein accumulated in the plasma membrane only at DOG concentrations >200 μM (Fig. 5 B). Thus, in living cells, the affinity of PKCε to bind either a membrane-permeable DAG analogue or the endogenous DAG species formed by PLC-β or -γ is indeed higher than that of the classical PKCα.

When PKCε–YFP/PKCα–CFP-coexpressing cells were incubated with 20 μM DOG for >1 min, PKCε slowly accumulated in the plasma membrane, indicating that the number of accessible DOG molecules was just sufficient to anchor the available PKCε–YFP molecules. The subsequent photolysis of caged Ca^{2+} (intracellularly loaded *o*-nitrophenyl-EGTA) resulted in an immediate membrane translocation of PKCα. Coincident with the accumulation of the classical PKC in the plasma membrane, the DOG-bound PKCε–YFP was displaced by >50% (Fig. 6, A and B). The observed displacement of PKCε became less efficient after extended coincubation with DOG, although PKCα–CFP was efficiently translocated in response to Ca^{2+} pulses (Fig. 6 B, middle and right). Similarly, a displacement of PKCε by Ca^{2+}-driven membrane association of PKCα did not occur when high DOG concentrations (100–200 μM) were applied (unpublished data). We conclude that the Ca^{2+}-driven displacement of DAG-bound PKCε is restricted to situations in which the number of accessible DAG molecules in the inner leaflet of the plasma membrane is not in vast excess over the number of PKC molecules that compete for the DAG binding. Because a pretreatment with bisindolylmaleimide I (1 μM for 15 min) did not prevent the displacement of DOG-bound PKCε by coexpressed PKCα (unpublished data), the competitive effect does not rely on the catalytic activity of coexpressed PKC isoforms.

To monitor the localization of individually expressed PKC isoforms during photolysis of caged Ca^{2+}, PKCε–CFP and PKCα–YFP were separately transfected into different cell populations and were then mixed and seeded on one coverslip. In cells that expressed only PKCε–CFP, the novel isoform again slowly translocated upon addition of DOG (20 μM), but a photolysis of Ca^{2+} failed to displace the DOG-bound PKCε (Fig. 6 C). The Ca^{2+} pulse, however, was sufficient because a robust translocation could be observed in PKCα–YFP-expressing cells located within the same visual field (Fig. 6 C). Thus, the competitive effect depends on a Ca^{2+}-driven membrane translocation of PKCα within the same cell. In the absence of exogenous DOG, the Ca^{2+} pulse selectively induced a translocation of PKCα–CFP and did not affect the localization of PKCε–YFP (Fig. 6 D).

Up to this point, the competition for DAG binding was observed at high PKC expression levels. This competitive mechanism may also operate at more physiological conditions with lower PKC expression levels and weaker PLC stimulation. We therefore generated a stably transfected $HEK_{PKC\varepsilon–YFP}$ cell line that typically expresses ~10-fold lower amounts of PKCε–YFP per cell than transiently transfected cells. Cells were stimulated with carbachol (100 μM) acting on an endogenously expressed M_1 family muscarinic acetylcholine receptor. This treatment caused a markedly weaker plasma membrane association of PKCε–YFP as compared with maximal stimulation via a cotransfected H_1 receptor (Fig. 7 A). Another estimate to quantify the phosphatidyl-4,5-bisphosphate (PIP_2) breakdown by stimulation of the endogenously expressed M_1 receptor was based on the membrane dissociation of a PIP_2- and $InsP_3$-binding YFP-fused PLCδ1 PH domain. The results confirm a remaining 20% PIP_2 hydrolysis as compared with stimulation of the transiently coexpressed H_1 receptor (unpublished data). As expected from the positive local feedback of $InsP_3$ and Ca^{2+} at $InsP_3$ receptors, the reduced input into the PLC signaling cascade was still sufficient to generate large $[Ca^{2+}]_i$ signals with peak values of 300–700 nM (Fig. 7 B), which clearly exceed threshold values for the Ca^{2+}-driven translocation of PKCα. $HEK_{PKC\varepsilon–YFP}$ cells were again transfected with various amounts of a PKCα–CFP-encoding cDNA plasmid. Furthermore, the molar ratios between stably expressed PKCε–YFP and transiently expressed PKCα–CFP were determined at the single-cell level. The transient coexpression of PKCα–CFP concentration-dependently suppressed the carbachol-induced plasma membrane docking of PKCε–YFP. This reduction was ~70% at an ~1:1 molar ratio, and saturation of the inhibitory effect was evident at a threefold molar excess of PKCα–CFP over PKCε–YFP (Fig. 7 C).

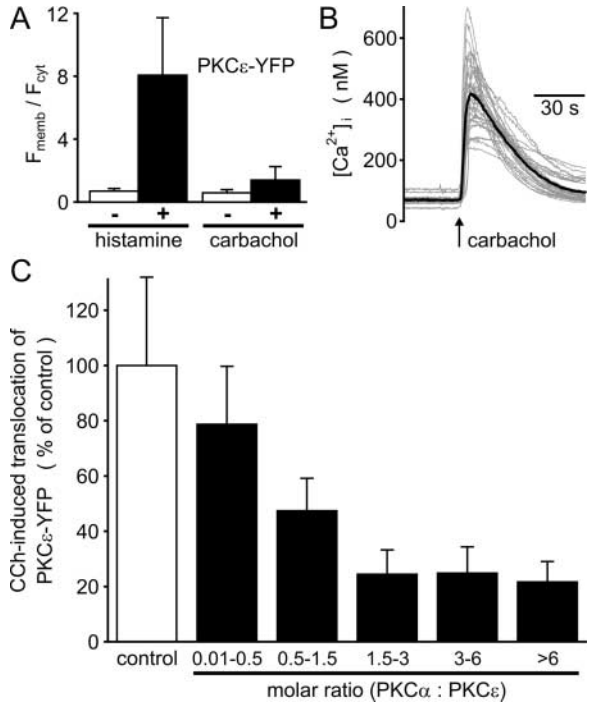

Figure 7. **PKCα concentration dependently suppresses the receptor-induced translocation of stably expressed PKCε.** (A) A HEK cell line that stably expresses low levels of PKCε–YFP ($HEK_{PKC\varepsilon–YFP}$) was generated and transfected with the H_1 histamine receptor. Cells were stimulated with either histamine (100 μM) or carbachol (100 μM; acting via an endogenous muscarinic receptor) as indicated. The plasma membrane association of PKCε–YFP was assessed before (open bars) and 20 s after agonist application (black bars) by confocal line-scan microscopy as described in Fig. 5. Data of three to six cells per experiment were averaged and expressed as means and SEM of four independent experiments. (B) Carbachol (100 μM)-induced $[Ca^{2+}]_i$ signals were determined in fura-2–loaded single $HEK_{PKC\varepsilon–YFP}$ cells (gray lines). The mean $[Ca^{2+}]_i$ is superimposed (black line). (C) $HEK_{PKC\varepsilon–YFP}$ cells were again transfected with PKCα–CFP. An endogenous muscarinic receptor was stimulated with carbachol (CCh; 100 μM), and PKC translocation was assessed as described in Fig. 3. The maximal translocation of PKCε–YFP in response to the agonist was normalized to cells that did not express additional PKCα–CFP (open bar). Molar ratios of PKCα and PKCε expression were calculated from the fluorescence intensities of the differently tagged PKC fusion proteins in single cells, and cells were grouped as indicated. Data represent means and SEM of seven independent transfection and imaging experiments.

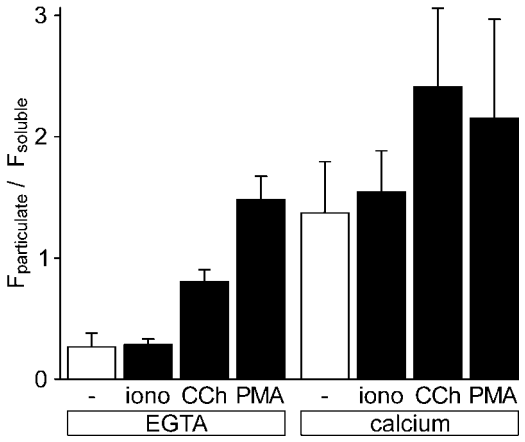

Figure 8. **Extraction of PKCα–YFP in the absence or presence of Ca^{2+}.** HEK cells were stably transfected with YFP-fused PKCα. After treating cells with either buffer (−), ionomycin (iono; 10 μM, 2 min), carbachol (CCh; 100 μM, 15 s) or PMA (10 μM, 5 min). Cells were lysed in either Ca^{2+}-free (nominally Ca^{2+}-free buffer supplemented with 0.5 mM EGTA) or Ca^{2+}-containing (1 mM) extraction buffers as indicated. Soluble and particulate fractions were separated and analyzed by fluorescence spectroscopy to obtain the ratio of fluorescence intensities ($F_{particulate}/F_{soluble}$). Data represent means and SEM of four independent extraction experiments.

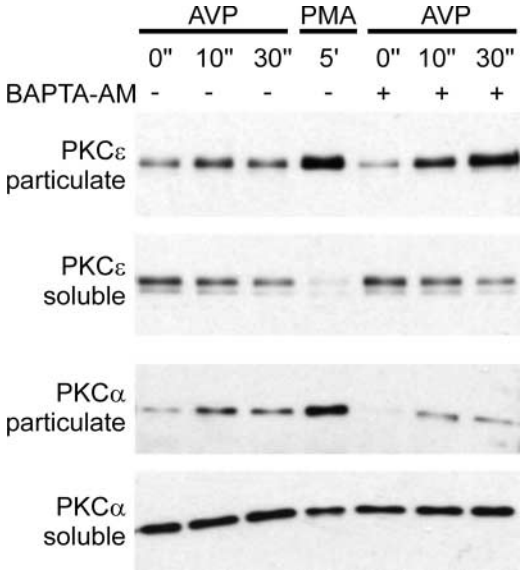

Figure 9. **The translocation of PKCα and PKCε in vascular smooth muscle cells is controlled in a Ca^{2+}-dependent manner.** Neonatal rat AoSMCs were pretreated with or without BAPTA-AM and subsequently stimulated with AVP (1 μM) for the indicated times. Particulate and soluble fractions were probed for endogenously expressed PKCα and PKCε as indicated. PMA stimulation (10 μM, 5 min) was included as a control.

Although imaging experiments were instrumental in defining the competitive translocation mechanism, translocation of endogenous PKCs is commonly quantified by Western blot analysis of PKCs in soluble and particulate cell fractions. The moderate appearance of PKCα–YFP in the particulate fraction of carbachol-stimulated HEK cells (Fig. 8) is not in agreement with the robust translocation seen in imaging experiments. The distribution of classical PKCs to soluble or particulate fractions strongly depended on the extraction method. Stimulation of HEK cells with carbachol (100 μM) or ionomycin (10 μM) in a Ca^{2+}-containing buffer resulted in a weak redistribution to the particulate fraction when extracts were prepared in Ca^{2+}-free media. In Ca^{2+}-containing extraction buffers, however, the classical PKCα was mainly found in the particulate fraction, even in the absence of the agonist (Fig. 8). As expected, the PKC activator PMA (10 μM for 5 min) redistributed PKCα–YFP to the particulate fraction in both extraction media. Thus, secondary redistribution during extraction precludes a determination of DAG-anchored fractions of the classical PKC isoforms. It may, therefore, be advantageous to study the competitive mechanism by monitoring the distribution of the novel PKCε that docks to DAGs in a Ca^{2+}-independent manner. The translocation of endogenously expressed PKCα as a competitor can hereby be favored or suppressed by intracellularly loaded BAPTA.

The competitive DAG binding of endogenously expressed PKC isoenzymes was assessed in neonatal rat aortic smooth muscle cells (AoSMCs) that express PKCα, PKCβ2 (trace amounts), PKCδ, and PKCε, as detected by immunoblot analysis (unpublished data). Incubation with PMA almost quantitatively translocated PKCε but only partially distributed PKCα to the particulate fraction, indicating that the stability of the interaction between the phorbol ester and the classical PKC is lower. After stimulation of an endogenously expressed V_1 vasopressin receptor with arginine-vasopressin (AVP; 1 μM) for 10 or 30 s, both PKCα and PKCε were partially distributed to the particulate fraction. The selected time points correspond to the observed maximal translocation of fluorescent PKCα and PKCε fusion proteins in transiently transfected and AVP-stimulated AoSMCs (unpublished data). In BAPTA-loaded cells, the stimulation with AVP failed to translocate PKCα, whereas translocation of the PKCε isoform was more efficient in BAPTA-loaded cells (Fig. 9). Thus, elevated $[Ca^{2+}]_i$ does not only support the agonist-induced translocation of classical PKCs, but also inversely affects the DAG binding of a novel PKC. This observation supports the concept that a competitive binding of classical and novel PKCs to DAGs contributes to a selective plasma membrane recruitment of PKC isoforms.

Discussion

Coimaging of fluorescent fusion proteins revealed that a selective plasma membrane recruitment of classical and novel PKC isoforms can result from a Ca^{2+}-controlled competitive binding to the lipid second messenger DAG. Without additional $[Ca^{2+}]_i$ signals, PKCε displayed a higher DAG binding affinity than PKCα, resulting in a selective plasma membrane translocation of the novel PKC isoform. By contrast, in the presence of $[Ca^{2+}]_i$ signals, classical PKCs bind to the plasma membrane with a diffusion-limited kinetic. Being redistributed to a two-dimensional plasma membrane compartment, the local increase of PKCα concentration within the target compartment is sufficient to occupy a majority of accessible DAG molecules and thereby prevents or displaces the DAG binding of novel PKCs. The Ca^{2+}-controlled competitive translocation of classical versus novel PKC iso-

forms was also detectable at physiological expression levels. This mechanism may enable a cell to decode stimuli by a directed membrane translocation and activation of distinct PKC isoforms.

Imaging of fluorescent PKC fusion proteins has provided a more realistic impression of the dynamics of these signaling molecules (Sakai et al., 1997; Feng and Hannun, 1998; Feng et al., 1998; Almholt et al., 1999; Codazzi et al., 2001). Most strikingly, the repetitive translocation of classical PKCs during oscillatory $[Ca^{2+}]_i$ responses was only detectable using these techniques (Oancea and Meyer, 1998; Dale et al., 2001; Schaefer et al., 2001). Currently available data on subtype-specific translocations of PKC isoforms predominantly rely on Western blot analyses of particulate and soluble cell fractions. This approach, however, does not necessarily reflect the distribution of PKCs at a given time point. In particular, during subcellular fractionation, classical PKCs may lose their membrane attachment (Kiley et al., 1990; Fig. 8). A secondary loss of membrane contact of classical PKCs during fractionation may result from (a) release of classical PKCs that are bound solely through a Ca^{2+}-dependent interaction with phosphatidylserine and/or (b) a low affinity of classical PKCs for DAG binding, which is not sufficient to maintain the membrane-bound state if additional stabilization by Ca^{2+} is lost. The contribution of both mechanisms may be indirectly inferred from the capability of Ca^{2+}-bound classical PKCs to prevent the DAG binding of the novel isoforms. Indeed, when $[Ca^{2+}]_i$ was clamped to resting concentrations (50–80 nM), translocation of PKCα was impaired whereas PKCε appeared to access DAGs more easily.

In living cells, several lines of evidence point to a higher DAG binding affinity of PKCε as compared with PKCα. Low concentrations of membrane-permeable DOG preferentially recruited PKCε to the plasma membrane. Second, receptor stimulation in BAPTA-loaded cells effectively translocated PKCε, but not coexpressed PKCα, and, in vascular smooth muscle cells, PMA treatment resulted in a complete translocation of endogenous PKCε, whereas the redistribution of PKCα was only partial. The DAG binding of recombinantly expressed and purified PKC isoenzymes has been determined using phorbol esters as DAG surrogates. Both absolute and relative binding affinities of different PKC isoforms, however, strongly depend on the lipid composition and the dispersion technique to generate artificial membranes (Kazanietz et al., 1993; Dimitrijevic et al., 1995). Therefore, reconstitution experiments do not necessarily reflect the DAG binding of PKC isoforms in living cells. Despite its inability to estimate absolute affinities, simultaneous imaging of PKC isoforms in living cells can be applied to compare the DAG binding of different PKC isoenzymes within their physiological environment. Another advantage of imaging versus extraction experiments is the coverage of the entire time course of a receptor-induced PKC redistribution. Co-imaging of classical and novel PKCs now revealed that the translocation of the classical isoforms precedes the maximum of the membrane anchorage of novel isoforms. For a given cell type and agonist, the observation of selective translocations of PKC isoforms is, therefore, not only influenced by extraction techniques but also by the choice of the incubation time.

The Ca^{2+}-controlled competitive translocation of classical and novel PKCs represents a mechanism by which signal diversification may emerge downstream of receptor activation. Although stimulation of PLC-coupled receptors commonly induces both $[Ca^{2+}]_i$ and DAG signals, their relative contribution to the PKC translocation underlies additional regulation. The catalytic activity of phosphoinositide-specific PLCs cleaves PIP_2 to form equimolar amounts of DAGs and $InsP_3$. In contrast to the direct interaction of DAGs with PKCs, $InsP_3$ action additionally depends on the filling state and responsiveness of internal Ca^{2+} stores. Refractory Ca^{2+} stores have been demonstrated to result from $InsP_3$ receptor downregulation (Wojcikiewicz and Nahorski, 1991; Bokkala and Joseph, 1997; Willars et al., 2001) or from a cGMP-dependent phosphorylation of IRAG, an $InsP_3$ receptor-associated cGMP kinase substrate (Schlossmann et al., 2000). Furthermore, owing to the biphasic effect of Ca^{2+} and ATP on $InsP_3$ receptor gating, $InsP_3$ can only operate at certain cytosolic conditions (Mak et al., 1998, 1999).

A competition for DAG binding of classical and novel PKCs requires that the number of accessible DAG molecules is limiting. Our data demonstrate that the Ca^{2+}-induced displacement of DOG-bound PKCε by PKCα is restricted to low concentrations of the membrane-permeable DAG analogue. The number of DAG molecules that are formed upon receptor stimulation can be roughly estimated. The $InsP_3$ receptor is fully activated in the presence of 10^{-8} to 10^{-7} M $InsP_3$ (Mak et al., 1998), which corresponds to a number of 12,000–120,000 molecules in a given cell of 2 picoliter volume. In various cell types, phorbol ester binding experiments have revealed a number of 40,000–800,000 binding sites per cell (Trilivas and Brown, 1989; Obeid et al., 1990; Combadière et al., 1993). Although these binding sites presumably include other DAG receptors, such as PKD, chimaerins, Munc13-1, or Ras-GRP, the total number of DAG acceptors, including classical and novel PKCs, appears not to be in vast excess over the number of DAGs formed during receptor stimulation.

From measurements of the total cellular DAG, one can calculate that a single cell contains 5×10^5 to 10^8 DAG molecules (Kiley et al., 1991; Baldassare et al., 1992). The high basal values and the modest increases upon receptor stimulation indicate that a major fraction of the total DAG content cannot be accessible for PKCs. A more detailed analysis has revealed that in resting cells, DAGs with saturated or monounsaturated fatty acids are predominant, whereas PLC activity mainly forms polyunsaturated DAG species, and the hypothesis that distinct DAG species, rather than changes in the total DAG mass, regulate PKC has been raised (Eskildsen-Helmond et al., 1998; Ivanova et al., 2001). A delayed formation of DAGs in the absence of $[Ca^{2+}]_i$ signals has been attributed to the catalytic activities of phosphatidylcholine-specific PLCs or PLDs. Whether this second wave of DAG formation leads to PKC activation is still under debate (Pettitt et al., 1997). Furthermore, PKC, via a noncatalytic pathway, is regarded as an activator of PLD activity rather than a target of PLD-induced DAG formation (Singer et al., 1996; Zhang et al., 1999). Consistent with the idea that second messengers formed by PLC activity may be scavenged by heterologously expressed

proteins, a modified $InsP_3$ receptor fragment, the "$InsP_3$ sponge," has only recently been introduced as a transfectable tool that intracellularly captures $InsP_3$ and prevents the agonist-induced Ca^{2+} mobilization from internal stores (Uchiyama et al., 2002). Kinase-dead PKC isoforms have been considered as dominant negative modulators of endogenous pathways (Ohba et al., 1998; Matsumoto et al., 2001; Braz et al., 2002). Although competition of kinase-dead and wild-type PKCε for receptor for activated C-kinases binding has been demonstrated (Pass et al., 2001), the dominant negative mechanism is far from being clarified. Our data suggest that dominant negative effects of overexpressed PKCs may also result from scavenging the accessible DAG molecules.

In contrast to experimental settings, physiological responses to hormones or paracrine stimuli have to decode slight changes in agonist concentrations that cause only submaximal receptor occupancy and weaker DAG formation. Therefore, competitive processes between DAG-binding signaling molecules are likely to occur in vivo. The highly efficient Ca^{2+}-driven plasma membrane association of classical PKCs and the superior DAG binding affinity of the novel PKCε represent a finely tuned system where $[Ca^{2+}]_i$ serves as a switch for the subtype-selective activation of PKCs. As a consequence, the competitive and/or sequential isotype-specific PKC activation is one of the mechanisms through which specific physiological responses may emerge from the signaling network of PKCs.

Materials and methods

Cell culture and transfections

HEK293 and primary cultures of rat embryonic AoSMCs (Reusch et al., 2001) were grown in MEM (Biochrom) supplemented with 10% FCS, penicillin (50 U/ml), and streptomycin (50 U/ml). Cells were seeded on 6-cm dishes and transfected the following day at 50–70% confluency with a Fugene 6 transfection reagent (Roche Molecular Biochemicals) and 4 μg of total plasmid cDNA per well according to the manufacturer's recommendations. After 18–24 h, cells were trypsinized and seeded on glass coverslips. All experiments were conducted 48–72 h after transfection. For selection and maintenance of the stably transfected $HEK_{PKC\varepsilon-YFP}$ cell line, the culture medium was supplemented with G418 (750 μg/ml). Vascular smooth muscle cells were starved in serum-free culture medium for 1 d before the experiments.

Generation of fluorescent PKC fusion proteins and fluorescence imaging

PKCα, β1, and ε were COOH-terminally fused to YFP in a custom-made pcDNA3-YFP fusion plasmid as described earlier (Schaefer et al., 2001). CFP fusions were generated analogous to the YFP-fused PKCs but using a custom-made pcDNA3-CFP vector that contains the open reading frame of enhanced CFP (Invitrogen) instead of enhanced YFP. Fluorescence imaging was performed with a monochromator and a cooled CCD camera (TILL-Photonics) connected to an inverted epifluorescence microscope (Axiovert 100; Carl Zeiss MicroImaging, Inc.). A 505-nm dichroic mirror (inflection point) with extended reflectivity (300–500 nm) was combined with a 510-nm long pass filter allowing coimaging of fura-2, CFP, and YFP signals. All imaging experiments were performed in a Hepes-buffered solution (HBS) containing 128 mM NaCl, 6 mM KCl, 1 mM $MgCl_2$, 1 mM $CaCl_2$, 5.5 mM glucose, 10 mM Hepes (pH 7.4), and 0.2% (wt/vol) BSA. Excitation spectra (320–490 nm) of single fluorochromes were taken either in untransfected HEK cells loaded with 4 μM fura-2AM (Molecular Probes) or in cells transiently expressing either CFP or YFP. Fura-2–loaded cells were equilibrated for 3 h in HBS supplemented with 10 μM ionomycin and 10 mM Ca^{2+} or 10 mM EGTA instead of Ca^{2+} in order to record excitation spectra of Ca^{2+}-bound fura-2 or free fura-2, respectively. Spectra were taken for each fluorochrome, dichroic mirror, and objective used in this study. Reference spectra were stored after subtracting background signals and normalizing the data to the maximal intensity of each dye. For coimaging of fluorescent proteins and $[Ca^{2+}]_i$, HEK cells were loaded with 2–4 μM fura-2AM for 30 min at 37°C. To obtain a measure for the membrane translocation of PKC isoenzymes, regions of interest were defined over the outer border (typical thickness of regions, 1–2 μm) and over the cytosol of a cell as shown in Fig. 3 A. Fluorescence intensities over the expected localization of the plasma membrane were averaged (F_{memb}) and divided by the mean fluorescence intensity over the cytosol of the same cell (F_{cyt}). To detect agonist-induced changes in the plasma membrane association, the resulting ratios were normalized to the initial values.

Confocal imaging of CFP- and YFP-fused PKCs was performed with an LSM510 inverted laser scanning microscope and a 63x/1.4 Plan-Apochromat objective (Carl Zeiss MicroImaging, Inc.). CFP was excited with the 458-nm line of an argon laser, and emitted light was collected with a 470–500-nm band pass filter. YFP was excited with the 488-nm laser line, and emission was recorded with a 530–560-nm band pass filter. For photolysis of caged Ca^{2+}, cells were loaded with 10 μM *o*-nitrophenyl-EGTA-AM (Molecular Probes; 40 min at 25°C), washed, and incubated for another 30 min in HBS before the experiment. Caged Ca^{2+} was photolyzed in defined areas by briefly switching the 364-nm line of an argon laser to maximal intensity. Pinholes were adjusted to yield optical sections of 0.7–1.4 μm.

Regression-based spectral evaluation of multiple fluorochromes

At any combination of excitation and emission wavelengths *i*, the background-corrected signal of the probe F_i is additively composed of fluorescences emitted from *m* different dyes $f_{i,m}$: $F_i = \Sigma(f_{i,1} \ldots f_{i,m})$. Because $f_{i,m}$ scales with both the unknown relative concentration of the dye c_m and its normalized fluorescence intensity at the chosen wavelength settings $x_{i,m}$ (Fig. 1 A), the term $f_{i,m} = c_m x_{i,m}$ dissects known ($x_{i,m}$) and unknown (c_m) parts. The signal of the probe can be described as $F_i = \Sigma(c_1 x_{i,1} \ldots c_m x_{i,m})$ (Fig. 1, B and C). The determination of fluorescence intensities of the probe at *n* different combinations of excitation and/or emission wavelengths provides *n* independent solutions for F_i. The resulting linear systems of equations can be solved if the number of different spectral settings *n* equals or exceeds the number of unknown relative dye concentrations $c_1..c_m$ (provided that linear dependence between the solutions can be excluded). For best reliability, we solved overdetermined ($n > m$) linear systems of equations by means of multivariate, constrained ($c_1..c_m \geq 0$), linear regression analyses:

$$\begin{bmatrix} c_1 \\ c_2 \\ c_3 \\ . \\ . \\ c_m \end{bmatrix} = \begin{bmatrix} \Sigma x_{i1}x_{i1} & \Sigma x_{i1}x_{i2} & \Sigma x_{i1}x_{i3} & . & . & \Sigma x_{i1}x_{im} \\ \Sigma x_{i2}x_{i1} & \Sigma x_{i2}x_{i2} & \Sigma x_{i2}x_{i3} & . & . & \Sigma x_{i2}x_{im} \\ \Sigma x_{i3}x_{i1} & \Sigma x_{i3}x_{i2} & \Sigma x_{i3}x_{i3} & . & . & \Sigma x_{i3}x_{im} \\ . & . & . & . & . & . \\ . & . & . & . & . & . \\ \Sigma x_{im}x_{i1} & \Sigma x_{im}x_{i2} & \Sigma x_{im}x_{i3} & . & . & \Sigma x_{im}x_{im} \end{bmatrix}^{-1} \begin{bmatrix} \Sigma x_{i1}F_i \\ \Sigma x_{i2}F_i \\ \Sigma x_{i3}F_i \\ . \\ . \\ \Sigma x_{im}F_i \end{bmatrix}$$

As a result, the relative concentrations of free ($c_{fura\text{-}2}$) and the Ca^{2+}-bound fura-2 ($c_{Ca\text{–}fura\text{-}2}$) are known, and interfering signals of GFP variants are eliminated. Therefore, the equation $[Ca^{2+}]_i = 224\ nM \times c_{Ca\text{-}fura\text{-}2}/c_{fura\text{-}2}$ can be applied to calibrate $[Ca^{2+}]_i$. The regression analysis was repeated for each image pixel at any time point resulting in a spatially and/or temporally resolved calibration of the $[Ca^{2+}]_i$ and in a dissection of signals arising from coexpressed CFP- and YFP-fused proteins. Furthermore, the molar ratio between CFP- and YFP-tagged fusion proteins can be assessed at the single-cell level. Based on the equimolar expression of CFP and YFP in an intramolecularly fused CFP–YFP tandem protein, a compensation for the lower fluorescence intensity of CFP could be calibrated. In our optical system used for coimaging of $[Ca^{2+}]_i$, CFP, and YFP, the fluorescence of YFP (c_{YFP}) appeared 8.1-fold brighter than for the intramolecularly coupled CFP (c_{CFP}; as detected after complete disruption of fluorescence resonance energy transfer by YFP photobleaching). Thus, the term c_{YFP}:$8.1 \times c_{CFP}$ corresponds to the molar ratio between coexpressed YFP- and CFP-fused proteins.

Cell fractionation and immunoblotting

For detection of PKCs in cytosolic and particulate fractions, cells were homogenized by two 5-s pulses of sonification (Branson sonifier) in an ice-cold lysis buffer containing 25 mM Tris/HCl, pH 7.5, 2 mM EDTA, 0.5 mM EGTA, 1 mM DTT, 200 μM phenylmethylsulfonyl fluoride and leupeptin/aprotinin (20 μg/ml each). Particulate material was removed (30,000 *g*, 20 min at 4°C), and supernatants representing the soluble PKC fractions were collected. The pellets were resuspended in lysis buffer supplemented with

1% (wt/vol) Triton X-100, sonified (5 s), and placed on a rocking platform (20 min at 4°C). Supernatants of a second centrifugation (30,000 *g*, 20 min at 4°C) were assigned as particulate PKC fraction. For immunoblotting, samples were diluted in Laemmli buffer containing 10% β-mercaptoethanol and subjected to a 10% SDS-PAGE. Separated proteins were electroblotted on nitrocellulose membranes, blocked in PBS containing 5% nonfat dry milk, and probed with polyclonal rabbit anti-PKCα or anti-PKCε antisera (1:1,000 in PBS; BD Biosciences) and a secondary, peroxidase-coupled anti–rabbit IgG antibody (Sigma-Aldrich). Chemiluminescence was detected with a Lumiglo reagent (New England Biolabs, Inc.).

The expression levels of endogenously expressed PKC isoenzymes and of heterologously expressed PKC fusion proteins were assessed in cytosolic fractions prepared from quiescent cells. 20 μg of protein or diluted samples of the transiently overexpressing cells were loaded on the gel. The transfection efficiency in these experiments was >50%, as detected by counting the total number and number of fluorescent cells.

We thank Claudia Plum for expert technical assistance and Daniel Sinnecker (Institut für Pharmakologie) for imaging PLC activity.

This study was supported by the Deutsche Forschungsgemeinschaft and the Fonds der Chemischen Industrie.

Submitted: 11 March 2002
Revised: 19 September 2002
Accepted: 19 September 2002

References

Almholt, K., P.O. Arkhammar, O. Thastrup, and S. Tullin. 1999. Simultaneous visualization of the translocation of protein kinase Cα-green fluorescent protein hybrids and intracellular calcium concentrations. *Biochem. J.* 337:211–218.

Baldassare, J.J., P.A. Henderson, D. Burns, C. Loomis, and G.J. Fisher. 1992. Translocation of protein kinase C isozymes in thrombin-stimulated human platelets. *J. Biol. Chem.* 267:15585–15590.

Bokkala, S., and S.K. Joseph. 1997. Angiotensin II-induced down-regulation of inositol trisphosphate receptors in WB rat liver epithelial cells. *J. Biol. Chem.* 272:12454–12461.

Braz, J.C., O.F. Bueno, L.J. De Windt, and J.D. Molkentin. 2002. PKCα regulates the hypertrophic growth of cardiomyocytes through extracellular signal–regulated kinase1/2 (ERK1/2). *J. Cell Biol.* 156:905–919.

Codazzi, F., M.N. Teruel, and T. Meyer. 2001. Control of astrocyte Ca^{2+} oscillations and waves by oscillating translocation and activation of protein kinase C. *Curr. Biol.* 11:1089–1097.

Combadière, C., E. Pedruzzi, J. Hakim, and A. Périanin. 1993. A protein kinase inhibitor, staurosporine, enhances the expression of phorbol dibutyrate binding sites in human polymorphonuclear leucocytes. *Biochem. J.* 289: 695–701.

Dale, L.B., A.V. Babwah, M. Bhattacharya, D.J. Kelvin, and S.S. Ferguson. 2001. Spatial-temporal patterning of metabotropic glutamate receptor-mediated inositol 1,4,5-triphosphate, calcium, and protein kinase C oscillations. *J. Biol. Chem.* 276:35900–35908.

Dekker, L.V., and P.J. Parker. 1994. Protein kinase C – a question of specificity. *Trends Biochem. Sci.* 19:73–77.

Dimitrijevic, S.M., W.J. Ryves, P.J. Parker, and F.J. Evans. 1995. Characterization of phorbol ester binding to protein kinase C isotypes. *Mol. Pharmacol.* 48: 259–267.

Eskildsen-Helmond, Y.E., D. Hahnel, U. Reinhardt, D.H. Dekkers, B. Engelmann, and J.M. Lamers. 1998. Phospholipid source and molecular species composition of 1,2-diacylglycerol in agonist-stimulated rat cardiomyocytes. *Cardiovasc. Res.* 40:182–190.

Feng, X., and Y.A. Hannun. 1998. An essential role for autophosphorylation in the dissociation of activated protein kinase C from the plasma membrane. *J. Biol. Chem.* 273:26870–26874.

Feng, X., J. Zhang, L.S. Barak, T. Meyer, M.G. Caron, and Y.A. Hannun. 1998. Visualization of dynamic trafficking of a protein kinase C βII/green fluorescent protein conjugate reveals differences in G protein-coupled receptor activation and desensitization. *J. Biol. Chem.* 273:10755–10762.

Ivanova, P.T., B.A. Cerda, D.M. Horn, J.S. Cohen, F.W. McLafferty, and H.A. Brown. 2001. Electrospray ionization mass spectrometry analysis of changes in phospholipids in RBL-2H3 mastocytoma cells during degranulation. *Proc. Natl. Acad. Sci. USA.* 98:7152–7157.

Jaken, S., and P.J. Parker. 2000. Protein kinase C binding partners. *Bioessays.* 22: 245–254.

Kazanietz, M.G., L.B. Areces, A. Bahador, H. Mischak, J. Goodnight, J.F. Mushinski, and P.M. Blumberg. 1993. Characterization of ligand and substrate specificity for the calcium-dependent and calcium-independent protein kinase C isozymes. *Mol. Pharmacol.* 44:298–307.

Kiley, S., D. Schaap, P.J. Parker, L.L. Hsieh, and S. Jaken. 1990. Protein kinase C heterogeneity in GH_4C_1 rat pituitary cells. *J. Biol. Chem.* 265:15704–15712.

Kiley, S.C., P.J. Parker, D. Fabbro, and S. Jaken. 1991. Differential regulation of protein kinase C isozymes by thyrotropin-releasing hormone in GH_4C_1 cells. *J. Biol. Chem.* 266:23761–23768.

Liu, W.S., and C.A. Heckman. 1998. The sevenfold way of PKC regulation. *Cell. Signal.* 10:529–542.

Mak, D.O., S. McBride, and J.K. Foskett. 1998. Inositol 1,4,5-trisphosphate activation of inositol trisphosphate receptor Ca^{2+} channel by ligand tuning of Ca^{2+} inhibition. *Proc. Natl. Acad. Sci. USA.* 95:15821–15825.

Mak, D.O., S. McBride, and J.K. Foskett. 1999. ATP regulation of type 1 inositol 1,4,5-trisphosphate receptor channel gating by allosteric tuning of Ca^{2+} activation. *J. Biol. Chem.* 274:22231–22237.

Matsumoto, M., W. Ogawa, Y. Hino, K. Furukawa, Y. Ono, M. Takahashi, M. Ohba, T. Kuroki, and M. Kasuga. 2001. Inhibition of insulin-induced activation of Akt by a kinase-deficient mutant of the ε isozyme of protein kinase C. *J. Biol. Chem.* 276:14400–14406.

Mellor, H., and P.J. Parker. 1998. The extended protein kinase C superfamily. *Biochem. J.* 332:281–292.

Nalefski, E.A., and A.C. Newton. 2001. Membrane binding kinetics of protein kinase C βII mediated by the C2 domain. *Biochemistry.* 40:13216–13229.

Nishizuka, Y. 1992. Intracellular signaling by hydrolysis of phospholipids and activation of protein kinase C. *Science.* 258:607–614.

Oancea, E., and T. Meyer. 1998. Protein kinase C as a molecular machine for decoding calcium and diacylglycerol signals. *Cell.* 95:307–308.

Obeid, L.M., T. Okazaki, L.A. Karolak, and Y.A. Hannun. 1990. Transcriptional regulation of protein kinase C by 1,25-dihydroxyvitamin D_3 in HL-60 cells. *J. Biol. Chem.* 265:2370–2374.

Ohba, M., K. Ishino, M. Kashiwagi, S. Kawabe, K. Chida, N.H. Huh, and T. Kuroki. 1998. Induction of differentiation in normal human keratinocytes by adenovirus-mediated introduction of the η and δ isoforms of protein kinase C. *Mol. Cell. Biol.* 18:5199–5207.

Pass, J.M., Y. Zheng, W.B. Wead, J. Zhang, R.C. Li, R. Bolli, and P. Ping. 2001. PKCε activation induces dichotomous cardiac phenotypes and modulates PKCε-RACK interactions and RACK expression. *Am. J. Physiol. Heart Circ. Physiol.* 280:H946–H955.

Pettitt, T.R., A. Martin, T. Horton, C. Liossis, J.M. Lord, and M.J. Wakelam. 1997. Diacylglycerol and phosphatidate generated by phospholipases C and D, respectively, have distinct fatty acid compositions and functions. *J. Biol. Chem.* 272:17354–17359.

Reusch, H.P., M. Schaefer, C. Plum, G. Schultz, and M. Paul. 2001. Gβγ mediate differentiation of vascular smooth muscle cells. *J. Biol. Chem.* 276:19540–19547.

Ron, D., and M.G. Kazanietz. 1999. New insights into the regulation of protein kinase C and novel phorbol ester receptors. *FASEB J.* 13:1658–1676.

Sakai, N., K. Sasaki, N. Ikegaki, Y. Shirai, Y. Ono, and N. Saito. 1997. Direct visualization of the translocation of the γ-subspecies of protein kinase C in living cells using fusion proteins with green fluorescent protein. *J. Cell Biol.* 139: 1465–1476.

Schaefer, M., N. Albrecht, T. Hofmann, T. Gudermann, and G. Schultz. 2001. Diffusion-limited translocation mechanism of protein kinase C isotypes. *FASEB J.* 15:1634–1636.

Schlossmann, J., A. Ammendola, K. Ashman, X. Zong, A. Huber, G. Neubauer, G.X. Wang, H.D. Allescher, M. Korth, M. Wilm, et al. 2000. Regulation of intracellular calcium by a signalling complex of IRAG, IP_3 receptor and cGMP kinase Iβ. *Nature.* 404:197–201.

Shao, X., B.A. Davletov, R.B. Sutton, T.C. Sudhof, and J. Rizo. 1996. Bipartite Ca^{2+}-binding motif in C2 domains of synaptotagmin and protein kinase C. *Science.* 273:248–251.

Singer, W.D., H.A. Brown, X. Jiang, and P.C. Sternweis. 1996. Regulation of phospholipase D by protein kinase C is synergistic with ADP-ribosylation factor and independent of protein kinase activity. *J. Biol. Chem.* 271:4504–4510.

Sutton, R.B., and S.R. Sprang. 1998. Structure of the protein kinase Cβ phospholipid-binding C2 domain complexed with Ca^{2+}. *Structure.* 6:1395–1405.

Trilivas, I., and J.H. Brown. 1989. Increases in intracellular Ca^{2+} regulate the

binding of [^{3}H]phorbol 12,13-dibutyrate to intact 1321N1 astrocytoma cells. *J. Biol. Chem.* 264:3102–3107.

Uchiyama, T., F. Yoshikawa, A. Hishida, T. Furuichi, and K. Mikoshiba. 2002. A novel recombinant hyper-affinity inositol 1,4,5-trisphosphate (IP_3) absorbent traps IP_3, resulting in specific inhibition of IP_3-mediated calcium signaling. *J. Biol. Chem.* 277:8106–8113.

Verdaguer, N., S. Corbalan-Garcia, W.F. Ochoa, I. Fita, and J.C. Gómez-Fernández. 1999. Ca^{2+} bridges the C2 membrane-binding domain of protein kinase Cα directly to phosphatidylserine. *EMBO J.* 18:6329–6338.

Wetsel, W.C., W.A. Khan, I. Merchenthaler, H. Rivera, A.E. Halpern, H.M. Phung, A. Negro-Vilar, and Y.A. Hannun. 1992. Tissue and cellular distribution of the extended family of protein kinase C isoenzymes. *J. Cell Biol.* 117:121–133.

Willars, G.B., J.E. Royall, S.R. Nahorski, F. El-Gehani, H. Everest, and C.A. McArdle. 2001. Rapid down-regulation of the type I inositol 1,4,5-trisphosphate receptor and desensitization of gonadotropin-releasing hormone-mediated Ca^{2+} responses in αT3–1 gonadotropes. *J. Biol. Chem.* 276:3123–3129.

Wojcikiewicz, R.J., and S.R. Nahorski. 1991. Chronic muscarinic stimulation of SH-SY5Y neuroblastoma cells suppresses inositol 1,4,5-trisphosphate action. *J. Biol. Chem.* 266:22234–22241.

Zhang, Y., Y.M. Altshuller, S.M. Hammond, F. Hayes, A.J. Morris, and M.A. Frohman. 1999. Loss of receptor regulation by a phospholipase D1 mutant unresponsive to protein kinase C. *EMBO J.* 18:6339–6348.